

pubs.acs.org/JPCB Article

Approximate Corona Phase Hamiltonian for Individual Cylindrical Nanoparticle-Polymer Interactions

Daniel James Lundberg and Michael S. Strano*



Cite This: J. Phys. Chem. B 2022, 126, 347-354



ACCESS I

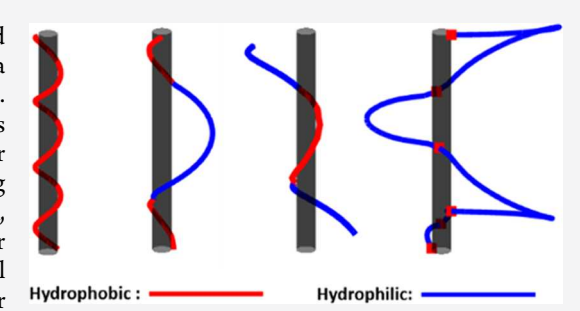
Metrics & More

Article Recommendations



Supporting Information

ABSTRACT: Nanoparticle surfaces, such as cylindrical nanowires and carbon nanotubes, are commonly coated with adsorbed polymer corona phases to impart solution stabilization and to control molecular interactions. These adsorbed polymer molecules (biological or otherwise), also known as the corona phase, are critical to engineering particle and molecular interactions. However, the prediction of its structure and the corresponding properties remains an unresolved problem in polymer physics. In this work, we construct a Hamiltonian describing the adsorption of an otherwise linear polymer to the surface of a cylindrical nanorod in the form of an integral equation summing up the energetic contributions corresponding to polymer bending, confinement, solvation, and electrostatics. We introduce an



approximate functional that allows for the solution of the minimum energy configuration in the strongly bound limit. The functional is shown to predict the pitch and surface area of observed helical corona phases in the literature based on the surface binding energy and persistence length alone. This approximate functional also predicts and quantitatively describes the recently observed ionic strength-mediated phase transitions of charged polymer corona at carbon nanotube surfaces. The Hamiltonian and the approximate functional provide the first theoretical link between the polymer's mechanical and chemical properties and the resulting adsorbed phase configuration and therefore should find widespread utility in predicting corona phase structures around anisotropic nanoparticles.

INTRODUCTION

A theoretical framework that is capable of predicting the adsorbed configuration of a polymer on a surface is fundamental to understanding the properties and behavior such functionalization imparts. While polymer adsorption onto flat surfaces is well studied,1 the polymer configuration on curved surfaces is strongly dependent on the surface's radius of curvature. Monte Carlo simulations have been used to develop phase diagrams for homopolymer adsorption to spherical surfaces, where the extent of adsorption and the resulting configurations are governed by the spherical radius. Configurations on ellipsoidal and cylindrical surfaces have been predicted using worm-like chain models³ and coarse-grained bead-and-spring models^{4,5} and through energetic scaling analysis, self-consistent field theory simulations, and experiments.8 Further, the conformational reconfiguration or desorption from these surfaces brought about by external chemical, electrical, or thermal stimuli is also important for understanding how particles interact for nanoparticle drug delivery,9 carbon nanotube-polymer composites,10 and organic solar cells.¹¹ The structure of an adsorbed polymer phase around a nanoparticle can also facilitate molecular recognition and binding, 12 enable nanoparticle separation and purification, 13,14 and allow interfacing with biological systems. 15-17

However, there is a dearth of understanding about the adsorbed polymer configuration at nanoparticle surfaces, particularly for cylindrical particles. The prediction of which polymers will adsorb onto a given cylindrical nanoparticle and the configuration of adsorbed polymer molecules on these nanoparticles remains difficult. Even for the comparatively well-characterized system of single-stranded DNA (ssDNA) on single-walled carbon nanotubes—which are used to separate nanotubes by size and chirality 14 and produce molecular recognition constructs 18—sequences that will bind to certain nanotube surfaces and the properties these adsorbed molecules impart remain poorly understood.

In this work, we develop a theoretical framework to describe the configuration of an adsorbed single polymer chain on a nanoscale cylindrical surface. We begin by proposing a Hamiltonian to describe the energy of a polymer chain interacting with the surface of a nanocylinder and use the calculus of variations to derive energetic criteria to predict

Received: November 22, 2021 Revised: December 8, 2021 Published: December 28, 2021





which linear homopolymer chains will uniformly adsorb onto a nanocylinder surface. Further, we find energy-minimizing configurations of a single adsorbed polymer to a nanocylinder surface. We find that the helical polymer configurations we predict match well with available imaging 19 and data on observed thermodynamic phase transitions 20,21 of such systems. Finally, the developed framework is expanded beyond the prediction of homopolymer configurations to the unique configurations of several hydrophobic-hydrophilic block copolymers. While this work solves only the solution for the configuration of a single chain, we emphasize that cases may exist where the configuration of multiple mutually interacting chains can be understood only through treating more than one chain at a time. It is our hope that the single-chain solution will serve as a basis to craft innovative multi-chain descriptions that are more tractable than current methods.

METHODS

We employ a worm-like chain model and consider an achiral polymer whose backbone is represented by the regular Cartesian space curve: $r(s) = [g_1(s)\vec{x}; g_2(s)\vec{y}; g_3(s)\vec{z}]$, as shown in Figure 1a. This polymer is adsorbed, partially or fully,

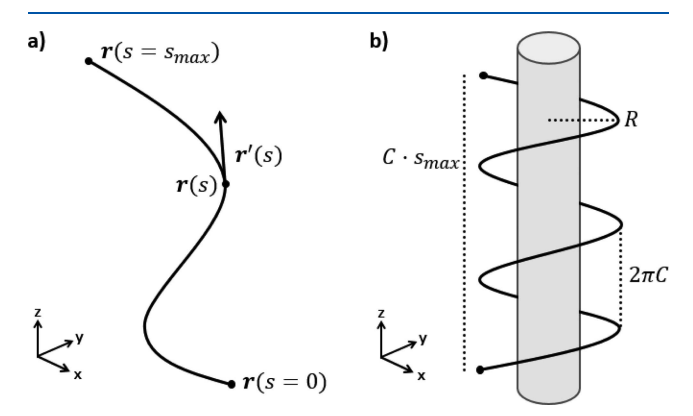


Figure 1. (a) General space curve in Cartesian coordinates. (b) General helical configuration of a polymer around a nanocylinder, with the helical radius, R, and pitch, $2\pi C$, wrapping a cylinder of radius $R_{\rm cyl}$. Helical configurations represent one subset of configurations that may be adopted from polymer adsorption to a nanocylinder surface.

on an infinite achiral cylinder with the longitudinal axis aligned along \vec{z} , as shown in Figure 1b. Bold terms in this work represent three vectors, with the arrow notation representing unit vectors. For a regular space curve, ||r'|| > 0 everywhere, and s, the parametric variable ranges from 0 to some upper value s_{\max} to trace the full chain. Because the polymer's configuration is not necessarily radially symmetric in general, Cartesian coordinates are maintained—facilitating the extension of the approach to non-cylindrical nanoparticles such as the sphere or platelet. The polymer contour length, L, is constant

$$L = \int_0^{s_{\text{max}}} ||r'|| \mathrm{d}s \tag{1}$$

For simplicity, we take the space curve to be parameterized by arc length (as is possible for any regular space curve), defining ||r'|| = 1 and $s_{\max} = L$.

A general Hamiltonian for the chain under interaction with a nanocylinder surface is as follows:

$$H = H_{\text{curvature}} + H_{\text{torsion}} + H_{\text{extension}} + H_{\text{adsorption}} + H_{\text{solvation}} + H_{\text{external}}$$
(2)

This has energetic contributions from the chain's curvature (bending), torsion, any enthalpic contribution from lengthening of the chain's backbone under high extensional force, ²² adsorption to the nanoparticle surface, ²³ polymer—solvent interactions, and last the contribution from any externally applied force on the chain.

For this work, the general Hamiltonian is simplified to neglect contributions from torsion, leading to a significant reduction in problem complexity (see further discussion in the Supporting Information). This assumption is justified in that incorporation of torsional rigidity is found to have a negligible effect on the behavior of worm-like chains in solution.2-However, it is noted that for the case of ssDNA interacting with chiral carbon nanotubes, spontaneous torsional rigidity is responsible for small but important energetic contributions which allow for chiral recognition, 25,26 and such contributions may be included in the presented approach if necessary. Double-stranded DNA and other highly torsionally rigid polymers deviate from this approximation and should be considered by accounting for these energy contributions. Additionally, chains are not extended beyond their original contour length, and the resulting enthalpic effects are ignored. The reduced Hamiltonian becomes

$$H = H_{\text{curvature}} + H_{\text{adsoprtion}} + H_{\text{solvation}} + H_{\text{external}}$$
(3)

For a worm-like chain, the energetic contribution from curvature, $H_{\rm curvature}$, is given as

$$H_{\text{curvature}} = k_{\text{B}}T \int_{0}^{s_{\text{max}}} \frac{1}{2} l_{\text{p}}(\kappa)^{2} ds$$
 (4)

where κ is the chain's curvature, defined for an arc-length parameterized curve as

$$\kappa = \|r''\| \tag{5}$$

where $l_{\rm p}$ is the persistence length and $k_{\rm B}T$ is the product of the Boltzmann constant and temperature. The contributions from polymer adsorption onto the cylindrical surface and solvation are incorporated as a single lumped surface interaction in the form of a Lennard-Jones potential

$$\begin{split} H_{\text{adsorption}} + H_{\text{solvation}} \\ &= \int_{0}^{s_{\text{max}}} V(r) \mathrm{d}s \\ &= \int_{0}^{s_{\text{max}}} \varepsilon_{\text{l}} \left[\left(\frac{r_{\text{m}}}{\|r - (r \cdot \vec{r}_{\text{cyl}})\| - R_{\text{cyl}}} \right)^{12} \right. \\ &\left. - 2 \left(\frac{r_{\text{m}}}{\|r - (r \cdot \vec{r}_{\text{cyl}})\| - R_{\text{cyl}}} \right)^{6} \right] \mathrm{d}s \end{split}$$

where $\varepsilon_{\rm l}$ and $r_{\rm m}$ are the depth of the potential well and the cylinder—chain distance where the potential takes this minimum value, respectively. The bending energy and this energy of attraction correspond to an implicit treatment of solvent—polymer and solvent—nanocylinder interactions. The above potential also takes into account solvation effects, where the depth of the potential energy well applied corresponds to the difference in energy between a fraction or

whole chain adsorbed to the surface and the free polymer chain in solution. The employed persistence length incorporates solvation effects on the polymer also. ²⁸

Last, the energetic contribution from an external force acting on the chain, *F*, is found as the product of chain extension in the direction of the force

$$H_{\text{external}} = \int_0^{s_{\text{max}}} \frac{r'}{\|r'\|} \cdot F \, ds \tag{7}$$

The only force we consider acting on the polymer is an entropic restoring force which resists chain extension. ²⁹ Such a force is mechanical in original—as the ends of a given chain extend further and further apart, fewer configurations can be adopted by the chain. Extending the polymer reduces the entropy of the system and acts to increase the total energy of the chain. To capture this phenomenon, we employ a single-term modification to the traditional Marko and Siggia expression for a chain in 3D, ³⁰ where the magnitude of this restoring force is a function of persistence length and chain extension, given as the ratio of end-to-end distance, h, and total contour length, L,

$$h = ||r(0) - r(s_{\text{max}})|| \tag{8}$$

$$\zeta = \frac{h}{L} = \frac{\|r(0) - r(s_{\text{max}})\|}{L} \tag{9}$$

$$F_{\rm S}(\zeta) = \frac{k_{\rm B}T}{l_{\rm p}} \left(\zeta - \frac{1}{4} + \frac{1}{4(1-\zeta)^2} - \frac{3}{4}\zeta^2 \right)$$
 (10)

Many approximations exist for this force; we choose the above for simplicity accuracy. ³¹ Further discussion of this force is included in the Supporting Information. This restoring force acts in the direction opposite to chain extension, which we approximate as extension along the longitudinal axis of the nanocylinder—assigned to the *z*-direction—in the positive direction

$$F_{s}(\zeta) = F_{s}\vec{r}_{z} \tag{11}$$

The total energy of the chain is then given by the following functional:

$$H = \int_{0}^{s_{\text{max}}} \left[\left(k_{\text{B}} T \frac{l_{\text{P}}}{2} (\|r''\|)^{2} - \left(\frac{r'}{\|r'\|} \right) \cdot F_{\text{s}} \right) + V(r) \right] ds$$
 (12)

Space curves which minimize the value for the above energy functional are found through solution of the Euler–Lagrange equations for the functional in eq 12.³²

$$\frac{\partial f}{\partial r} + \sum_{k} (-1)^{k} \frac{\mathrm{d}^{k}}{\mathrm{d}s^{k}} \frac{\partial f}{\partial r^{(k)}} = 0$$
(13)

These, when applied to eq 12 for the x-, y-, and z-coordinates, are

$$\varepsilon_{x} = \frac{\partial V(r)}{\partial x} - \frac{\mathrm{d}}{\mathrm{d}s} \frac{\partial}{\partial x'} \left(-\frac{r'}{\|r'\|} \cdot F_{s} \right) + \frac{\mathrm{d}^{2}}{\mathrm{d}s^{2}} \frac{\partial}{\partial x''} \left(\frac{l_{p}}{2} (\|r''\|)^{2} \right)$$

$$= 0 \tag{14}$$

$$\varepsilon_{y} = \frac{\partial V(r)}{\partial y} - \frac{\mathrm{d}}{\mathrm{d}s} \frac{\partial}{\partial y'} \left(-\frac{r'}{\|r'\|} \cdot F_{\mathrm{S}} \right) + \frac{\mathrm{d}^{2}}{\mathrm{d}s^{2}} \frac{\partial}{\partial y''} \left(\frac{l_{\mathrm{p}}}{2} (\|r''\|)^{2} \right)$$

$$= 0 \tag{15}$$

$$\varepsilon_z = -\frac{\mathrm{d}}{\mathrm{d}s} \frac{\partial}{\partial z'} \left(-\frac{r'}{\|r'\|} \cdot F_{\mathrm{S}} \right) + \frac{\mathrm{d}^2}{\mathrm{d}s^2} \frac{\partial}{\partial z''} \left(\frac{l_{\mathrm{p}}}{2} (\|r''\|)^2 \right) = 0 \tag{16}$$

Any space curve which satisfies all three Euler–Lagrange equations above necessarily represents an energy extrema of eq 12, from which energy-minimizing configurations can be found. However, an adequate number of boundary conditions for the partial differential Euler–Lagrange equations are required to determine a unique energy-minimizing configuration. Ultimately, we choose to solve the Euler–Lagrange equations of eq 12 imposing the position of the Chain ends as boundary conditions, r(s=0) and $r(s=s_{\rm max})$, separated by some distance along the nanocylinder, which also impose a specific, constant entropic restoring force, $F_s(\zeta)$. In general, however, the Euler–Lagrange equations may be solved leaving one or both of these end points unspecified, requiring further optimization to obtain their position.

RESULTS

To begin, we determine the conditions under which a polymer molecule will favor adsorption to any nanocylinder surface through scaling analysis of ε_x and ε_y . The magnitude of the attraction modeled as the Lennard-Jones potential is compared against the contributions from curvature and entropic elasticity. In the regime where the attractive force dominates, we can say that uniform polymer adsorption is energetically favored.

Scalings for all terms in eqs 14 and 15 are chosen as follows: x and y scale as the radius of the nanocylinder, $R_{\rm cyl}$. For an arc length parameterized curve, $||\vec{r}'|| = 1$, and x' and y' scale as unity with the parametric variable, s, scaling as contour length, L. With curvature defined as $\kappa = ||r''||$, this value equals the reciprocal of the radius of curvature of the chain. Taking this radius of curvature to scale as the radius of the nanocylinder, the scaling of curvature and thus x'' and y'' is taken to be $R_{\rm cyl}^{-1}$. The entropic force resisting chain extension is approximated to scale as $l_{\rm p}^{-1}$. The attractive force between the chain and the cylinder surface is taken to scale as $\varepsilon_{\rm l}$. Note that because the scaling for x' and y', and x'' and y' are the same, the non-identical equations ε_x and ε_y scale identically.

When the energetic contribution from the entropic restoring force and curvature are negligible compared to that of the attraction between the polymer and nanotube surface, ε_x and ε_y are well approximated as

$$\varepsilon_x \approx \varepsilon_y \approx \frac{\partial V(r)}{\partial x} = 0$$
 (17)

This approximation is valid under the conditions

$$\frac{\varepsilon_{\rm l}}{k_{\rm B}T} \gg \frac{l_{\rm p}}{LR_{\rm cyl}} \tag{18}$$

$$\frac{\varepsilon_{\rm l}}{k_{\rm B}T} \gg \frac{l_{\rm p}}{L^2} \tag{19}$$

$$\frac{\varepsilon_{\rm l}}{k_{\rm B}T} \gg \frac{R_{\rm cyl}}{Ll_{\rm p}} \tag{20}$$

Inequalities eqs 18 and 19 represent scaling of the attractive force against that of curvature, and inequality eq 20 represents the scaling of this force against the force resisting chain

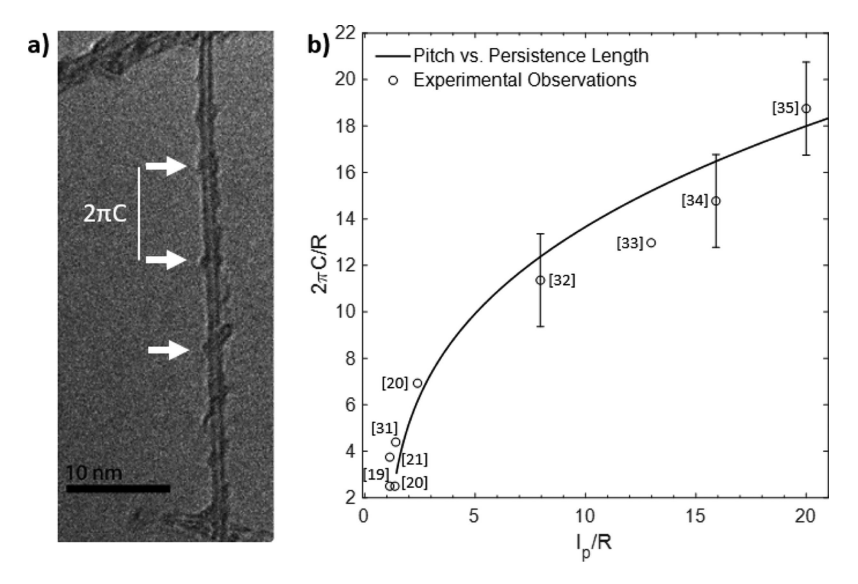


Figure 2. (a) TEM image of a PNES-wrapped carbon nanotube in aqueous solution. The polymer adopts a helical configuration around the less than 1 nm diameter carbon nanotube. The rigid polymer molecule enforces that the helical configuration is sparse, with a large pitch, nearing 10 nm. Reproduced with permission from Deria et al.³⁶ (P. Deria, L. E. Sinks, T. H. Park, D. M. Tomezsko, M. J. Brukman, D. A. Bonnell, M. J. Therien. Organic Solvent Solubility of Single-Walled Carbon Nanotubes Helically Wrapped by Ionic, Semiconducting Polymers. Nano Lett. 2010, 10, 4192. Copyright 2010 American Chemical Society). (b) Predicted helical pitch from polymer persistence length vs experimental observations of helically wrapped carbon nanotubes for the following polymers: ssDNA, ^{19–21} polyacetylene, ³⁷ PNES, ^{36,38} alginic acid, ³⁹ PPES, ⁴⁰ and chitosan. ⁴¹ Values are normalized against the helical radius to account for varying carbon nanotube diameters.

extension. When inequalities eqs 18-20 are satisfied, the polymer is approximated to be uniformly adsorbed to the nanocylinder surface.

Helical wrapping of individual polymer molecules around carbon nanotubes is one well-documented class of corona phase configurations which exist in this limit. This configuration is defined by two parameters: R, the helical radius, and C (taken to be positive), which sets the pitch (height of one complete turn) equal to $2\pi C$, as shown in Figure 2a. We note that this defines a right-handed helix and that the presented Hamiltonian contains no terms which favor either right-handed or left-handed wrapping on an achiral nanocylinder. The polymer's and/or nanotube's chirality will influence the favored direction of the helical configuration, as has been predicted for ssDNA in numerical simulation.³⁴ The general space curve is

$$r(s) = [R \operatorname{Cos}(s)\vec{x}; R \operatorname{Sin}(s)\vec{y}; Cs\vec{z}]$$
 (21)

When eqs 18–20 are satisfied, ε_x and ε_y reduce to eq 17 and are only satisfied when the helical radius becomes

$$R = R_{\rm cyl} + r_{\rm m} \tag{22}$$

Ultimately then, an energy-minimizing helical configuration exists only if ε_z can be satisfied at this radius, with ε_z becoming

$$-2l_{p}\frac{CR^{2}}{(R^{2}+C^{2})^{3}}+(F_{S}(\zeta))\left[\left(\frac{1}{\sqrt{R^{2}+C^{2}}}\right)\right]$$
$$-\left(\frac{C^{2}}{(R^{2}+C^{2})^{3/2}}\right)$$
$$=0$$
(23)

where

$$\zeta = \frac{C}{\sqrt{R^2 + C^2}}\tag{24}$$

 ε_z is a fourth-order differential equation requiring four initial or boundary conditions to produce a unique solution. Here, the helical radius and pitch uniquely define a single value of chain extension given a polymer contour length, L. This effectively enforces the pair of essential boundary conditions z(s=0)=0 and $z(s_{\max})=L\frac{C}{\sqrt{R^2+C^2}}$. The helical form also enforces that $z'(s=0)=z'(s=s_{\max})=C$.

The existence of an energy-minimizing helical configuration ultimately depends on the energetics of polymer-carbon nanotube interactions, the nanotube geometry, and the physical properties of the polymer: $\varepsilon_{\rm l}$, $r_{\rm m}$, and $l_{\rm p}$. For a range of experimentally and computationally measured helical configurations of a polymer on a cylinder, often reported in terms of the helical pitch adopted, the persistence length which would result in such a configuration can be found from eq 23 and compared to that polymer's known or estimated persistence length. These results are presented graphically in Figure 2b and tabulated in the Supporting Information. Agreement is seen between the predicted and both experimentally and computationally observed helical polymeric wrappings on carbon nanotube surfaces. We note that the chirality of the polymer and the nanotube around which it is configured will ultimately decide the preferred handedness of the helical wrapping, as would be the case for a polymer molecule possessing spontaneous torsion. Here, the experimental reports rely heavily on samples of chirally impure HiPCO or CoMoCAT single-walled carbon nanotube samples,³⁵ and chiral assignment of the nanotube-polymer composite when the helical pitch is measured is not always

As another test of the presented approach, we consider the separate problem of ionic strength-mediated phase transitions of ssDNA on carbon nanotube surfaces. Salem et al. reported a

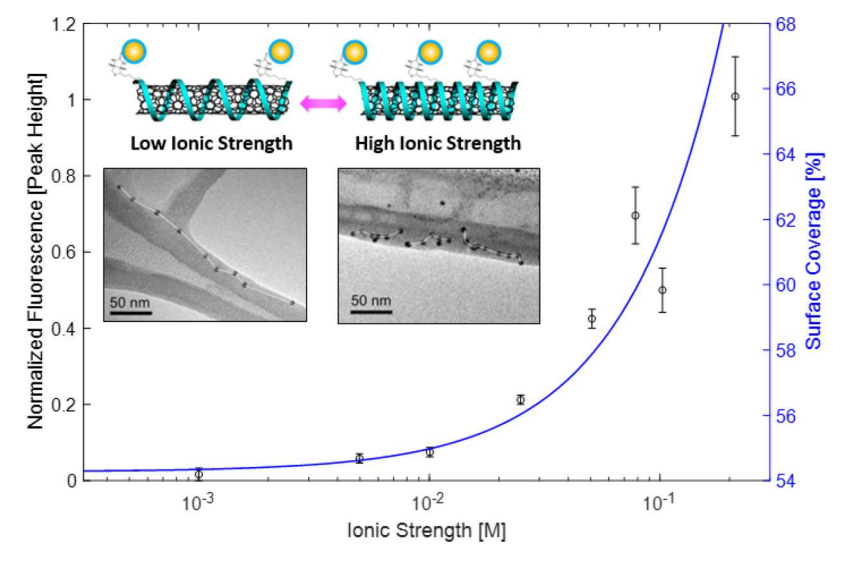


Figure 3. Ionic strength dependence of surface area coverage of a poly(T) helical wrapping compared to the concurrent fluorescence quenching of carbon nanotubes. The percent surface coverage of a ssDNA helical wrapping of a 0.8 nm diameter carbon nanotube is determined by treating the polymer as a 1 nm ribbon on the tube surface. Fluorescence data from carbon nanotubes wrapped in poly(T) at various ionic strengths in the presence of riboflavin are reported by Salem et al.²⁰ with error bars representing the standard deviation over three experimental measurements. Fluorescence tracks with the surface coverage provided by the wrapping—as the ionic strength increases, the effective persistence length of the poly(T) wrapping decreases, allowing for a tighter helical wrapping and increased surface area coverage. As the surface area coverage increases, there is less unexposed nanotube surface where riboflavin may bind and cause fluorescence quenching, which leads to higher total fluorescence. Inlay: visualization of the altered helical configuration of ssDNA wrapping carbon nanotubes. The TEM image shows gold nanoparticle-functionalized ssDNA molecules wrapping around carbon nanotubes. Reproduced with permission from Salem et al.²⁰ D. P. Salem, X. Gong, A. T. Liu, V. B. Koman, J. Dong, M. S. Strano. Ionic Strength-Mediated Phase Transitions of Surface-Adsorbed DNA on Single-Walled Carbon Nanotubes. J. Am. Chem. Soc. 2017, 139, 16791. Copyright 2017 American Chemical Society.

configurational phase change for poly(thymine) wrapping (poly(T)) from high surface coverage at high ionic strength to low coverage at low ionic strength (Figure 3 Inlay). This reconfiguration was monitored by measuring the relative separation of gold nanoparticles functionalized to both ends of ssDNA stands which wrapped the nanotube. Further, by exposing the ssDNA-wrapped carbon nanotube at various ionic strengths to the small molecule riboflavin, fluorescence quenching was observed as a result of riboflavin adsorption to the exposed surface of the nanotube where not covered by poly(T) strands. 18,42 We find that by expanding the presented model to include the ionic strength dependence of persistence length on poly(T) ssDNA, 43 we are able to accurately predict surface coverage of the wrapping as it tracks with ionic strength. By treating the ssDNA as a nanometer wide ribbon lying flat on the tube's surface, 44 we find that the ionicstrength-dependent fluorescence quenching shown by Salem et al. and the predicted surface coverage are in strong agreement, as shown in Figure 3, further validating the model's ability to describe the corona phase configuration and physical properties.

Helical wrappings represent only a single class of polymer configurations on cylindrical nanoscale surfaces—the variational approach introduced in this work is easily extended to more complex polymers through numerical solution of the Euler—Lagrange equations. To demonstrate this, we predict the configurations of several different polymer systems as shown in Figure 4. Here, the weak formulation of the Euler—Lagrange equations for the Hamiltonian under the isoperimetric constrain of eq 1 was solved using finite element analysis in COMSOL Multiphysics 5.5.

For example, an adherent homopolymer that produces a helical wrapping of a 15 nm pitch, as in Figure 4a, will produce

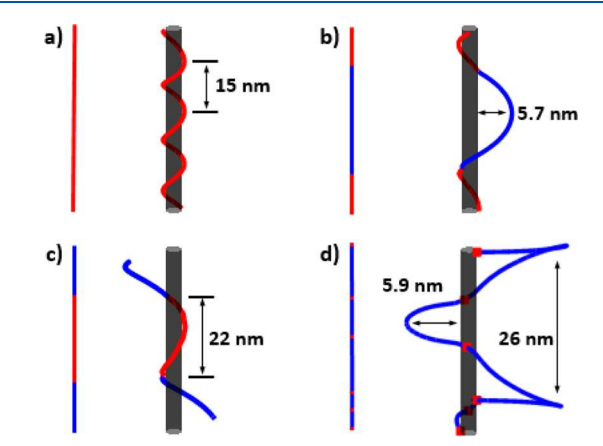


Figure 4. Examples of predicted polymer configurations upon interaction with a nanocylinder. All polymers are defined to have a contour length of 100 nm and a constant persistence length of 5 nm. Blue sections represent hydrophilic monomer units where $\varepsilon_1 = 0$. Red sections represent hydrophobic monomer units whose attractive force satisfied inequalities eqs 18-20. Polymers are configured around a nanocylinder of 1.5 nm diameter and 50 nm length. (a) Predicted homopolymer helical wrapping. (b) ABA hydrophobic-hydrophilichydrophilic block copolymer, consistent with rhodamine isothiocyanate-difunctionalized poly(ethylene glycol)-wrapped carbon nanotubes used for sensing applications. 18 (c) BAB hydrophilic hydrophobic-hydrophilic block copolymer representative of a poloxamer. 46 (d) Random copolymer with low-mole-fraction hydrophobic monomers such as methacrylic acid and styrene-containing copolymers, whose composites with carbon nanotubes have been used for the development of molecular recognition sensors. 4/,4

a 5.7 nm loop when an interior hydrophilic block is inserted at a constant total polymer length. This "anchor-loop" config-

uration has been observed indirectly via experiments and directly in explanatory molecular simulations¹⁸ and is consistent with a 2D equation of state description of the associated corona phase.⁴⁵ The predicted configuration in Figure 4b is consistent with a rhodamine isothiocyanatedifunctionalized poly(ethylene glycol) previously shown to readily disperse carbon nanotubes for sensing applications. 18 Inverting this triblock polymer with hydrophilic domains moved to the ends produces a centrally adsorbed corona phase consistent with that of a poloxamer or Pluronic polymer consisting of the polyethylene oxide (PEO)-polypropylene oxide (PPO)-polyethylene oxide (PEO) triblock polymer as shown in Figure 4c, where the predicted configuration agrees with recent simulations. 46 As a final example, Figure 4d shows a random copolymer of hydrophobic and hydrophilic moieties, with a low hydrophobic content. Such random hydrophobichydrophilic copolymers have found use in creating artificial recognition sights for hormones and pharmaceuticals. 47,48 Overall, we find that the inhomogeneity of energetic parameters on the level of individual blocks or monomers within a polymer chain allows for the generation of more finely tuned configurations upon interaction with the nanocylinder surface. Expanding this inhomogeneity to bending rigidity (as would be necessary to treat block copolymers with both rigid and more flexible blocks⁴⁹) to torsional rigidity or by introducing varying intrinsic torsion (as would be the case for a polymer with varying chirality along the backbone⁵⁰) will be able to expand the scope the presented model to a breadth of polymer chemical and physical architectures.

CONCLUSIONS

To conclude, in this work, we construct a Hamiltonian describing the adsorption of a single linear polymer to the surface of a cylindrical nanorod or nanotube in the limit of strong binding such that it can predict the resultant corona phase configuration—a longstanding challenge in nanotechnology. The resulting integral equation involving the energetic contributions corresponding to polymer bending, confinement, solvation, and electrostatics can be solved analytically or through numerical solution of the Euler-Lagrange formulation. The presented approach produces a range of energy-minimizing configurations of various hydrophilic and hydrophobic homo- and heteropolymers that match experimental and computational results in the literature to date. This corona phase Hamiltonian can describe the pitch and surface area of observed helical corona phases in the literature from the surface binding energy and persistence length. It also predicts and quantitatively describes recently observed ionic strength-mediated phase transitions of charged polymer corona at carbon nanotube surfaces. This Hamiltonian and its solution provide a much needed link between polymer mechanical and chemical properties and the resulting adsorbed phase configuration at the nanoparticle surface and therefore should find widespread utility in nanotechnology.

DATA AVAILABILITY

The data that support the findings of this study are available within the article and in its Supporting Information.

ASSOCIATED CONTENT

Supporting Information

The Supporting Information is available free of charge at https://pubs.acs.org/doi/10.1021/acs.jpcb.1c09998.

Further discussion on incorporation of torsional rigidity to the polymer model, summary of scaling of Euler—Lagrange equations, summary of physical characterization of helical wrappings from literature, further discussion on the helical configuration, further information about numerical simulation, and further discussion of entropic effects on the polymer configuration (PDF)

AUTHOR INFORMATION

Corresponding Author

Michael S. Strano — Department of Chemical Engineering, Massachusetts Institute of Technology, Cambridge, Massachusetts 02139, United States; orcid.org/0000-0003-2944-808X; Email: Strano@MIT.edu

Author

Daniel James Lundberg – Department of Chemical Engineering, Massachusetts Institute of Technology, Cambridge, Massachusetts 02139, United States

Complete contact information is available at: https://pubs.acs.org/10.1021/acs.jpcb.1c09998

Notes

The authors declare no competing financial interest.

ACKNOWLEDGMENTS

D. Lundberg acknowledges support from the National Science Foundation Graduate Research Fellowship under grant no. 1745302.

REFERENCES

- (1) Baschnagel, J.; Meyer, H.; Wittmer, J.; Kulić, I.; Mohrbach, H.; Ziebert, F.; Nam, G. M.; Lee, N. K.; Johner, A. Semiflexible Chains at Surfaces: Worm-Like Chains and beyond. *Polymers (Basel)* **2016**, *8*, 1.
- (2) Mansky, P.; Liu, Y.; Huang, E.; Russell, T. P.; Hawker, C. Controlling polymer-surface interactions with random copolymer brushes. *Science* **1997**, *275*, 1458.
- (3) Linse, P.; Källrot, N. Polymer adsorption from bulk solution onto planar surfaces: Effect of polymer flexibility and surface attraction in good solvent. *Macromolecules* **2010**, *43*, 2054.
- (4) Semenov, A. N.; Bonet-Avalos, J.; Johner, A.; Joanny, J. F. Adsorption of polymer solutions onto a flat surface. *Macromolecules* **1996**, 29, 2179.
- (5) Advincula, R.; Aust, E.; Meyer, W.; Knoll, W. In situ investigations of polymer self-assembly solution adsorption by surface plasmon spectroscopy. *Langmuir* **1996**, *12*, 3536.
- (6) Chakraborty, A. K.; Golumbfskie, A. J. Polymer Adsorption—Driven Self-Assembly of Nanostructures. *Annu. Rev. Phys. Chem.* **2001**, 52, 537–573.
- (7) Sheridan, R. J.; Orski, S. V.; Jones, R. L.; Satija, S. K.; Beers, K. L. Surface Interaction Parameter Measurement of Solvated Polymers via Model End-Tethered Chains. *Macromolecules* **2017**, *50*, 6668.
- (8) Flood, C.; Cosgrove, T.; Howell, I.; Revell, P. Effects of Electrolytes on Adsorbed Polymer Layers: Poly (ethylene oxide)-Silica System. *Langmuir* **2006**, *22*, 6923.
- (9) Urbina, M. C.; Zinoveva, S.; Miller, T.; Sabliov, C. M.; Monroe, W. T.; Kumar, C. S. S. R. Investigation of magnetic nanoparticle-polymer composites for multiple-controlled drug delivery. *J. Phys. Chem. C* **2008**, *112*, 11102.

- (10) Spitalsky, Z.; Tasis, D.; Papagelis, K.; Galiotis, C. Progress in Polymer Science Carbon nanotube—polymer composites: Chemistry, processing, mechanical and electrical properties. *Prog. Polym. Sci.* **2010**, *35*, *357*.
- (11) Nogueira, A. F.; Lomba, B. S.; Soto-Oviedo, M. A.; Correia, C. R. D.; Corio, P.; Furtado, C. A.; Hümmelgen, I. A. Polymer solar cells using single-wall carbon nanotubes modified with thiophene pedant groups. *J. Phys. Chem. C* **2007**, *111*, 18431.
- (12) Bisker, G.; Ahn, J.; Kruss, S.; Ulissi, Z. W.; Salem, D. P.; Strano, M. S. A Mathematical Formulation and Solution of the CoPhMoRe Inverse Problem for Helically Wrapping Polymer Corona Phases on Cylindrical Substrates. *J. Phys. Chem. C* **2015**, *119*, 13876–13886.
- (13) Johnson, R. R.; Kohlmeyer, A.; Johnson, A. T. C.; Klein, M. L.; Pennsyl, V.; Pennsyl, V. Free Energy Landscape of a DNA Carbon Nanotube Hybrid Using Replica Exchange Molecular Dynamics. *Nano Lett.* **2009**, *9*, 537–541.
- (14) Zheng, M.; Jagota, A.; Semke, E. D.; Diner, B. A.; McLean, R. S.; Lustig, S. R.; Richardson, R. E.; Tassi, N. G. DNA-assisted dispersion and separation of carbon nanotubes. *Nat. Mater.* **2003**, *2*, 338.
- (15) Kim, O.-K.; Je, J.; Baldwin, J. W.; Kooi, S.; Pehrsson, P. E.; Buckley, L. J. Solubilization of Single-Wall Carbon Nanotubes by Supramolecular Encapsulation of Helical Amylose. *J. Am. Chem. Soc.* **2003**, *125*, 4426.
- (16) Numata, M.; Asai, M.; Kaneko, K.; Bae, A.-H.; Hasegawa, T.; Sakurai, K.; Shinkai, S. Inclusion of Cut and As-Grown Single-Walled Carbon Nanotubes in the Helical Superstructure of Schizophyllan and Curdlan (β -1,3-Glucans). *J. Am. Chem. Soc.* **2005**, *127*, 5875.
- (17) Khalid, P.; Suman, V. B.; Hussain, M. A.; Arun, A. B. Toxicology of Carbon Nanotubes A Review. *Int. J. Appl. Eng. Res.* **2016**, *11*, 148–157.
- (18) Zhang, J.; Landry, M. P.; Barone, P. W.; Kim, J.-H.; Lin, S.; Ulissi, Z. W.; Lin, D.; Mu, B.; Boghossian, A. A.; Hilmer, A. J.; et al. Molecular recognition using corona phase complexes made of synthetic polymers adsorbed on carbon nanotubes. *Nat. Nanotechnol.* **2013**, *8*, 959.
- (19) Cathcart, H.; Nicolosi, V.; Hughes, J. M.; Blau, W. J.; Kelly, J. M.; Quinn, S. J.; Coleman, J. N. Ordered DNA Wrapping Switches on Luminescence in Single-Walled Nanotube Dispersions. *J. Am. Chem. Soc.* 2008, 130, 12734.
- (20) Salem, D. P.; Gong, X.; Liu, A. T.; Koman, V. B.; Dong, J.; Strano, M. S. Ionic Strength-Mediated Phase Transitions of Surface-Adsorbed DNA on Single-Walled Carbon Nanotubes. *J. Am. Chem. Soc.* **2017**, *139*, 16791.
- (21) Yarotski, D. A.; Kilina, S. V.; Talin, A. A.; Tretiak, S.; Prezhdo, O. V.; Balatsky, A. V.; Taylor, A. J. Scanning tunneling microscopy of DNA-Wrapped carbon nanotubes. *Nano Lett.* **2009**, *9*, 12.
- (22) Bouchiat, C.; Wang, M. D.; Allemand, J.-F.; Strick, T.; Block, S. M.; Croquette, V. Estimating the persistence length of a worm-like chain molecule from force-extension measurements. *Biophys. J.* **1999**, 76, 409.
- (23) Brunecker, F. K.; Schöppler, F.; Hertel, T. Interaction of Polymers with Single-Wall Carbon Nanotubes. *J. Phys. Chem. C* **2016**, 120, 10094.
- (24) Groot, R. D. Mesoscale simulation of semiflexible chains. I. Endpoint distribution and chain dynamics. *J. Chem. Phys.* **2013**, *138*, 224903.
- (25) Shankar, A.; Zheng, M.; Jagota, A. Energetic Basis of Single-Wall Carbon Nanotube Enantiomer Recognition by Single-Stranded DNA. *J. Phys. Chem. C* **2017**, *121*, 17479.
- (26) Lustig, S. R.; Jagota, A.; Khripin, C.; Zheng, M. Theory of structure-based carbon nanotube separations by Ion-exchange chromatography of DNA/CNT hybrids. *J. Phys. Chem. B* **2005**, *109*, 2559
- (27) Reddy, G.; Yethiraj, A. Implicit and Explicit Solvent Models for the Simulation of Dilute Polymer Solutions. *Macromolecules* **2006**, *39*, 8536.

- (28) Nakajima, K.; Watabe, H.; Nishi, T. Solvent Effects on Single Poly- mer Chain Physics Investigated by Atomic Force Microscopy. *Kautsch. Gummi Kunstst.* **2006**, *59*, 256–260.
- (29) Marko, J. F.; Siggia, E. D. Statistical mechanics of supercoiled DNA. *Phys. Rev. E* **1995**, *52*, 2912.
- (30) Ogden, R. W.; Saccomandi, G.; Sgura, I. Computational aspects of Worm-Like-Chain interpolation formulas. *Comput. Math. with Appl.* **2007**, *53*, 276.
- (31) Ortiz, C.; Hadziioannou, G. Entropic Elasticity of Single Polymer Chains of Poly(methacrylic acid) Measured by Atomic Force Microscopy. *Macromolecules* **1999**, *32*, 780.
- (32) Serfaty, S. Lagrange and the calculus of variations. *Lett. Mat.* 2014, 2, 39.
- (33) Filobello-Nino, U.; Vazquez-Leal, H.; Huerta-Chua, J.; Callejas-Molina, R. A.; Sandoval-Hernandez, M. A. A practical proposal to obtain solutions of certain variational problems avoiding Euler formalism. *Heliyon* **2020**, *6*, No. e03703.
- (34) Zerze, G. H.; Stillinger, F. H.; Debenedetti, P. G. The Handedness of DNA Assembly around Carbon Nanotubes Is Determined by the Chirality of DNA. *J. Phys. Chem. B* **2020**, *124*, 5362.
- (35) Komatsu, N.; Wang, F. A comprehensive review on separation methods and techniques for single-walled carbon nanotubes. *Materials* **2010**, *3*, 3818.
- (36) Deria, P.; Sinks, L. E.; Park, T.-H.; Tomezsko, D. M.; Brukman, M. J.; Bonnell, D. A.; Therien, M. J. Phase Transfer Catalysts Drive Diverse Organic Solvent Solubility of Single-Walled Carbon Nanotubes Helically Wrapped by Ionic, Semiconducting Polymers. *Nano Lett.* **2010**, *10*, 4192–4199.
- (37) Shan, M.; Xue, Q.; Lei, T.; Xing, W.; Yan, Z. Self-assembly of helical polyacetylene nanostructures on carbon nanotubes. *J. Phys. Chem. C* **2013**, *117*, 16248.
- (38) Bonhommeau, S.; Deria, P.; Glesner, M. G.; Talaga, D.; Najjar, S.; Belin, C.; Auneau, L.; Trainini, S.; Therien, M. J.; Rodriguez, V. Raman Spectroscopic Investigation of Individual Single-Walled Carbon Nanotubes Helically Wrapped by Ionic, Semiconducting Polymers. J. Phys. Chem. C 2013, 117, 14840–14849.
- (39) Liu, Y.; Chipot, C.; Shao, X.; Cai, W. Solubilizing Carbon Nanotubes through Noncovalent Functionalization. Insight from the Reversible Wrapping of Alginic Acid around a Single-Walled Carbon Nanotube. *J. Phys. Chem. B* **2010**, *114*, 5783.
- (40) Kang, Y. K.; Lee, O.-S.; Deria, P.; Kim, S. H.; Park, T.-H.; Bonnell, D. A.; Saven, J. G.; Therien, M. J. Helical Wrapping of Single-Walled Carbon Nanotubes by Water Soluble Poly (p-phenyleneethynylene). *Nano Lett* **2009**, *9*, 1414–1418.
- (41) Liu, Y.; Chipot, C.; Shao, X.; Cai, W. Free-Energy Landscape of the Helical Wrapping of a Carbon Nanotube by a Polysaccharide. *J. Phys. Chem. C* 2011, *115*, 1851.
- (42) Polo, E.; Kruss, S. Impact of Redox-Active Molecules on the Fluorescence of Polymer-Wrapped Carbon Nanotubes. *J. Phys. Chem.* C **2016**, *120*, 3061.
- (43) Chen, H.; Meisburger, S. P.; Pabit, S. A.; Sutton, J. L.; Webb, W. W.; Pollack, L. Ionic strength-dependent persistence lengths of single-stranded RNA and DNA. *Proc. Natl. Acad. Sci.* **2012**, *109*, 799–804.
- (44) Wang, H.; Tang, Z.; Li, Z.; Wang, E. Self-assembled monolayer of ssDNA on Au (111) substrate. Surf. Sci. 2001, 480, L389–L394.
- (45) Ulissi, Z. W.; Zhang, J.; Sresht, V.; Blankschtein, D.; Strano, M. S. 2D equation-of-state model for corona phase molecular recognition on single-walled carbon nanotube and graphene surfaces. *Langmuir* **2014**, *31*, 628.
- (46) Sarukhanyan, E.; Milano, G.; Roccatano, D. Coating mechanisms of single-walled carbon nanotube by linear polyether surfactants: Insights from computer simulations. *J. Phys. Chem. C* **2014**, *118*, 18069.
- (47) Dong, J.; Lee, M. A.; Rahaman, I.; Sun, J. H.; Govind, A.; Salem, D. P.; Strano, M. S. A Synthetic Mimic of Inhibitor Binding in Phosphodiesterase Type 5 based on Corona Phase Molecular

Recognition of Single Walled Carbon Nanotubes. *Proc. Natl. Acad. Sci.* **2018**, *117* (43), 26616–26625.

- (48) Lee, M. A.; Wang, S.; Jin, X.; Bakh, N. A.; Nguyen, F. T.; Dong, J.; Silmore, K. S.; Gong, X.; Pham, C.; Jones, K. K.; et al. Implantable Nanosensors for Human Steroid Hormone Sensing In Vivo Using a Self-Templating Corona Phase Molecular Recognition. *Adv. Healthcare Mater.* **2020**, *9*, 2000429.
- (49) Scherman, O. A.; Rutenberg, I. M.; Grubbs, R. H. Direct synthesis of soluble, end-functionalized polyenes and polyacetylene block copolymers. *J. Am. Chem. Soc.* **2003**, *125*, 8515.
- (50) Green, M. M.; Peterson, N. C.; Sato, T.; Teramoto, A.; Cook, R.; Lifson, S. A helical polymer with a cooperative response to chiral information. *Science* **1995**, *268*, 1860.

